RSC Advances

ROYAL SOCIETY OF CHEMISTRY

www.rsc.org/advances

Dissipative particle dynamics and experimental study of alkane-based nanoencapsulated phase change material for thermal energy storage

Zhonghao Rao[1,2]*, Yutao Huo[1], Xinjian Liu[1]

1 School of Electric Power Engineering, China University of Mining and Technology, Xuzhou 221116 China

2 Key Laboratory of Efficient Utilization of Low and Medium Grade Energy (Tianjin University), Ministry of Education of China, Tianjin 300072 China

Abstract

The nanoencapsulated phase change materials (PCM) for thermal energy storage have received much attention recently. In order to understand the morphologies and structure evolution of nanoencapsulated PCM, the dissipative particle dynamics (DPD) simulation coupled with experimental method were performed in this paper. The coarse-grained models of the alkane-based nanoencapsulated PCM system were constructed and the PCM nanocapsules were prepared by using n-octadecane as core material, methyl methacrylate (MMA) and methyl acrylate (MA) as shell materials. The results showed that the nanoencapsulated PCM with shell-core structure were successfully fabricated by DPD simulation. The average diameter of the prepared PCM capsules by using experiment method is 48.80 nm. The latent heat and melting temperature of the prepared nanoencapsulated PCM is 86.13 $kJ \cdot kg^{-1}$ and 20.60 ^{o}C. The alkane content in the prepared nanoencapsulated PCM is 41.59%. The DPD simulation method was confirmed to benefit the development of nanotechnology in thermal energy storage.

Keywords: Thermal energy storage, Nanoencapsulated phase change material, Dissipative particle dynamics, latent heat

* Corresponding author. Tel.: +86 516 83592000. E-mail address: raozhonghao@cumt.edu.cn.

1. Introduction

With the continuing fossil fuel consumption and growing environmental concerns, research and development of renewable and sustainable energy have received serious attention in recent years. Among all forms of energy, thermal energy is abundantly available such as solar thermal energy and geothermal resources, as well as waste heat from various man-made energy conversion systems [1]. Unfortunately, solar thermal energy varies significantly during the day and night [2], and most of the industrial waste heat suffer common disadvantages as intermittent and uncertainty [3]. Hence, there is no doubt that the storage of thermal energy will play an important role in adjusting the mismatch between the supply and demand.

Thermal energy storage may involve only sensible heat storage, latent heat storage or a combination of both [4]. One of thermal energy storage solutions proposed is using latent heat of phase change materials (PCM), which can store/release a large amount of heat during melting/solidification processes [5, 6]. In the past decades, enormous work has been carried out to explore the PCM-related preparation, characterization, performance improvement and applications. Moreover, there are dozens of review articles published in recent three years to summarize the PCM-related work, specifically, preparation, structure and properties [7], thermal performance enhancement [8, 9], integration in building [10, 11, 12], application in textiles and clothing systems [13],

battery thermal management [14], to name a few. In order to overcome the problems such as leak, reaction with the surrounding, low thermal conductivity and mechanical stability of PCM in thermal energy storage system, the encapsulation technique has been widely used to encapsulate PCM as macroencapsulated, microencapsulated and nanoencapsulated PCM [15, 16, 17, 18, 19]. Compared with macroencapsulated and microencapsulated PCM, the nanoencapsulated PCM with smaller particle size have significant advantage in some fields especially in latent functionally thermal fluids [20]. Although the concept of nanocapsule was presented in 1970s and the nanocapsulation technology has been widely developed, the precedence for producing nanoencapsulated PCM is still limited [20]. By using in situ polymerization, Zhang et al. [21] have fabricated a kind of nanoencapsulated PCM. Fang et al. [20] have synthesized the nanoencapsulated PCM with diameter of 100 nm to 123 nm. Fang et al. [22] have prepared the nanoencapsulated PCM with diameter of about 100 nm. While by miniemulsion polymerization, Li et al. [23] have synthesized the nanoencapsulated PCM with diameter of 253 to 285 nm. Chen et al. [24] have synthesized the nanoencapsulated PCM with mean diameter of 150 nm. Zhang et al. [19] have prepared the nanoencapsulated PCM with average size of 140 nm and 119 nm. Hong et al. [18] have made the nanoencapsulated PCM with average diameter of 200 nm using colloid method. It can be seen that the size and thermal performance of the fabricated nanoencapsulated PCM may be different due to the difference of preparation method and core and shell materials. Therefore, a computer simulation method for preliminary forecasting the performance of nanoencapsulated PCM from mesoscopic may be efficient and economical for experiment.

The development of dissipative particle dynamics (DPD) simulation method leads to a possibility to understand the nanoencapsulated PCM from mesoscopic. We have used DPD

simulation method to investigate the mesoscopic morphologies of microencapsulated PCM according to the results of other scholars [25]. Analogously, using the DPD method to discuss morphologies of nanoencapsulated PCM should not be ignored. For further understanding the microstructure changes of nanoencapsulated PCM and then benefiting for the experiment, in the present study, the alkane was used as core material and methyl methacrylate and methyl acrylate were used as shell materials to fabricate nanoencapsulated PCM by using DPD simulation coupled with experiment.

2. Modeling and experiment

Before the synthesized experiment, the DPD method was used to simulate the mesostructures and morphology evolution of the nano-encapsulated PCM. In the DPD simulations, n-octadecane, a kind of alkane, was used as core material. The methyl methacrylate (MMA) and methyl acrylate (MA) were used as shell materials. The azodiisobutyronitrile (AIBN) and sodium dodecyl sulfate (SDS) were used as surfactant. Fig. 1 shows the coarse-grained models of the nanoencapsulated PCM system. In the models, a group of molecules was represented as a DPD bead. It can be seen that each molecule of methyl methacrylate, methyl acrylate and azodiisobutyronitrile are represented as bead MMA, MA and AIBN, respectively. Six water molecules accumulated as a bead W. An n-octadecane molecule is divided into four beads C. And a sodium dodecyl sulfate molecule is divided into two beads C and a bead SO. The time evolution of motion for the above mentioned beads all obeys the Newton's equations of motion [26]:

$$\frac{dr_i}{dt} = v_i, m_i \frac{dv_i}{dt} = f_i \quad (1)$$

where f_i, m_i, r_i, and v_i are the force, mass, position vectors, and velocity vectors of bead i,

respectively. The forces between each pair of beads contain conservative force (F_{ij}^{C}), dissipative force (F_{ij}^{C}), random force (F_{ij}^{R}) and spring force (F_{ij}^{R}), which can be described as [27, 28]:

$$f_i = \sum_{j \neq i}(F_{ij}^{C} + F_{ij}^{D} + F_{ij}^{R} + F_i^{S}) \quad (2)$$

where,

$$F_{ij}^{C} = \begin{cases} -a_{ij}(1 - r_{ij}/r_c)\hat{\boldsymbol{r}}_{ij}, & r_{ij} < r_c \\ 0, & r_{ij} > r_c \end{cases} \quad (3)$$

$$F_{ij}^{D} = \frac{\sigma^2[\omega(r_{ij})]^2}{2kT}(\boldsymbol{v}_{ij} \cdot \hat{\boldsymbol{r}}_{ij})\hat{\boldsymbol{r}}_{ij} \quad (4)$$

$$F_{ij}^{R} = \frac{\sigma\omega(r_{ij})\hat{\boldsymbol{r}}_{ij}\xi}{\sqrt{\delta_t}} \quad (5)$$

$$F_i^{S} = \sum_j C\,\boldsymbol{r}_{ij} \quad (6)$$

where, $\boldsymbol{r}_{ij} = \boldsymbol{r}_i - \boldsymbol{r}_j$, $r_{ij} = |\boldsymbol{r}_{ij}|$, $\hat{\boldsymbol{r}}_{ij} = \boldsymbol{r}_{ij}/r_{ij}$, $\boldsymbol{v}_{ij} = \boldsymbol{v}_i - \boldsymbol{v}_j$. r_c is the cutoff radius. $\omega(r)$ stands for *r*-dependent weight function $\omega(r) = (1 - r)$ for *r* <1 and $\omega(r) = 0$ for *r* > 1. ξ is a random number with zero mean and unit variance. σ > 0 and δ_t is the time step. *C* is the spring constant. a_{ij} is the interaction parameter of bead *i* and *j*. For the same type of beads, the interaction parameter a_{ii} can be obtained as [29]:

$$a_{ii}\rho = 75k_BT \quad (7)$$

For the different type of beads, the interaction parameter a_{ij} can be obtained as [29]:

$$a_{ij} = a_{ii} + 3.27\chi_{ij} \quad (8)$$

where χ_{ij} denotes the Flory–Huggins parameter and can be obtained as [25]:

$$\chi_{ij} = \frac{V_{bead}}{kT}(\delta_i - \delta_j)^2 \quad (9)$$

where V_{bead} is the average molar volume of two beads. δ_i and δ_j denote the solubility parameters of bead *i* and *j*. In this paper, the simulated molar volumes and solubility parameters of different beads is shown in Table 1, and then the interaction parameters of different beads in the PCM system can be calculated and shown in Table 2.

To obtain the molar volumes and solubility parameters, preliminary molecular dynamics (MD) simulations were performed. The MD processes have been presented detailed in our previous study [30, 31, 32]. Take methyl methacrylate as an example, the smart minimization method and three annealing cycles were calculated to equilibrate single methyl methacrylate molecule and whole methyl methacrylate system. The energy and density fluctuating of methyl methacrylate is shown in Fig. 2. Then the equilibrated systems were calculated for long enough to obtain the molar volumes and solubility parameters. In the following DPD simulations, the cubic box with a size of 40 × 40 × 40 with periodic boundary conditions was adopted after excluded the influence of box sizes. The time step was taken as 0.05 and 200 000 steps were adopted to obtain equilibration phase. All the simulations were calculated using DPD program incorporated in the Materials Studio 5.5 software (Accelrys).

Based on the DPD simulated results, a preliminary proportion of shell and core materials of nanoencapsulated PCM can be obtained. The materials used in the experiment include ZDJN28 (85% n-octadecane, ShiJiaZhuang Rubitherm PCMS CO., LTD, China), MMA (Shanghai Lingfeng Chemical Reagent Co. Inc., China), MA (Sinopharm Chemical Reagent Co., Ltd., China), AIBN (Tianjin Kemiou Chemical Reagent Co., Ltd., China), SDS (Shanghai Lingfeng Chemical Reagent Co. Inc., China), aqueous sodium chloride (NaCl, Sinopharm Chemical Reagent Co., Ltd., China), ethanol (Sinopharm Chemical Reagent Co., Ltd., China) and petroleum ether solution (Chinasun Specialty Products Co., Ltd., China). The monomer mixture of MMA, MA and AIBN was added to the melted RT28 to obtain oil phase A. The surfactant (SDS) was dispersed in deionized water to obtain water phase B. Then the oil phase was added into the water phase and the mixture was pre-emulsified by a homogenizer at the stirring rate of 2000 rpm for 30 min in constant temperature

water bath (35 ^{o}C) to obtain the pre-emulsion. The pre-emulsion was added into a four necked flask with stirring rate of 300 rpm under nitrogen atmosphere at 70 ^{o}C of the constant temperature water bath. The reaction was carried out for 4 h and then the nanoencapsulated PCM mixture were cooled at room temperature under natural cooling. The nanoencapsulated PCM were demulsified by using the mixture of NaCl and ethanol, and then washed with petroleum ether solution for twice and deionized water for three times to remove the unencapsulated n-octadecane. Finally, the nanoencapsulated PCM were dried with vacuum oven for 12 h.

A particle size analyzer (NPA150, Microtrac Inc.) was used to measure the diameter of the nanoencapsulated PCM. The morphologies of the nanoencapsulated PCM were obtained by using a scanning electron microscopy (SEM ZEISS EVO 18, ZEISS) at an accelerated voltage of 10 kV. The thermal performance of the dried nanoencapsulated PCM were measured using a differential scanning calorimeter (DSC Q 20, TA Instruments) under N_2 atmosphere with scanning rate of 10 ^{o}C·min^{-1} in the temperature range of -10 ^{o}C to 50 ^{o}C.

3. Results and discussion

At first, to fabricate the nanoencapsulated PCM, the possible proportion of different materials including n-octadecane, MMA, MA, AIBN and SDS were determined according to the published results such as Fang et al. [20] (St/n-octadecane/AIBN = 10g/10g/0.1g), Fang et al. [22] (formaldehyde/n-tetradecane/SDS = 14g/15g/0.5g) and Chen et al. [24] (MMA/n-Dodecanol/AIBN/ DNS-86 = 10g/10g/0.2g/0.2-1.0g). In the PCM system, the proportion of MMA/MA/n-octadecane/ AIBN/SDS was adjusted by DPD simulations and then an acceptable ratio can be obtained after adjusted a few times. Fig. 3 shows the pressure, temperature and diffusivity evolution with

simulated time of the nanoencapsulated PCM, which have an optimized relative amount of MMA/MA/n-octadecane/AIBN/SDS as 100/10/100/1/3. The water content is sufficient in the PCM system. The total simulated time is 100 000 DPD units (200 000 steps). It can be seen that obvious changes of the pressure, temperature and diffusivity appear in the first 2000 DPD units. And then the pressure and temperature fluctuate within a certain range. The diffusivity of bead W did not change much after about 4000 DPD units. The reason is that the water provides a liquid environment and can not be encapsulated as shell and core of the nanoencapsulated PCM. The diffusivity of bead C, MMA, MA, AIBN and SO declined slowly to about zero until the last 2000 DPD units. It is indicated that different beads in the PCM systems reached equilibrium state especially at the last 2000 DPD units, that is, a time of 100 000 DPD units per simulation process is long enough to make the PCM system achieving simulation equilibrium.

It is no doubt that, to observe the spherical structure of nanoencapsulated PCM, the DPD system should achieve equilibrium state. While the system reached equilibrium state, the structure of the simulated PCM system may not be spherical. For further understanding the final state of the DPD simulated PCM system, the density concentration profiles and stress difference in the PCM system were shown in Fig. 4. The density of bead W from 10 DPD units to 35 DPD units showed a decreasing trend followed by increasing trend. While the trend of bead C showed an opposite trend with bead W, that is, the concentration of n-octadecane near 23 DPD units is the largest and the structure of n-octadecane should be spherical. In addition, the relative amount of n-octadecane/MMA is 1/1; while the density concentration of bead MMA did not show an obvious trend which is similar with bead C. It can be concluded that the structure of MMA should not be a solid sphere. According to the curve of stress difference, the final state of the PCM system should

be a spherical structure. Coupled with the density concentration curve of bead W and the stress difference curve of the whole PCM system, the only content in the PCM system from 0 to 7 DPD units must be water. The two peaks of the stress difference curve can be used to determine the interface of water and PCM sphere.

In order to determine the shell and core structure of the simulated PCM system, the morphology of the PCM sphere was presented. Fig. 5 shows the morphology of a capsule at t = 200 000 steps from the DPD simulations. The beads which used to represent n-octadecane phases are colored with green, MMA with blue, MA with magenta, W and SD with others. To display the morphology of the PCM sphere clearly, water molecules are not showed. From the cross-sectional view of the PCM sphere, it can be clearly seen that the n-octadecane were encapsulated with shell materials. Hence, the encapsulated PCM were fabricated by using DPD simulations.

In order to observe the dynamics process of encapsulated PCM in the DPD simulations, Fig. 6 shows the change of aggregates with increasing simulation steps in the simulated PCM system. Where, to observe more PCM capsules, the DPD simulation with a same proportion of different materials was performed in the cubic box with a size of 50 × 50 × 50. At first (Fig. 6a, t = 0 step), all beads are dispersed randomly in the box. At t= 2 000 step ((Fig. 6b), under the forces between each pair of beads, some n-octadecane molecules started to aggregate together. Some PCM sphere can be seen at t = 20 000 step (Fig. 6c). With the increase of simulated time (Fig. 6d and Fig. 6e), the obvious PCM capsules can be observed. And the morphology of the PCM capsules has not changed much from t = 100 000 step to t = 200 000 step. The above DPD simulations confirmed that the encapsulated PCM capsules were successfully fabricated with a possible proportion of MMA/MA/n-octadecane/ AIBN/SDS as 100/10/100/1/3.

Based on the DPD simulated results, the experiment with 5.5 g ZDJN28, 5 g MMA, 0.5 g MA, 0.05 g AIBN and 0.15 g SDS was performed to prepare nanoencapsulated PCM. Fig. 7 shows a scanning electron microscope (SEM) image and particle size distribution of the nanoencapsulated PCM. The spherical PCM capsules can be clearly observed. The tested average diameter (d_a) of the PCM capsules by particle size analyzer is 48.80 nm. That is, the size of a DPD simulated PCM capsule should be consistent with the experimental result. In other words, the nanoencapsulated PCM can be fabricated by the DPD simulations.

For the nanoencapsulated PCM, only the core materials absorb/release thermal energy during the heating/cooling process. The phase change temperature and latent heat can be determined by using differential scanning calorimeter (DSC). Fig. 8 shows the DSC curves of the nanoencapsulated PCM and the core material ZDJN28. It can be seen that the latent heat and melting temperature of ZDJN28 is 207.10 kJ·kg^{-1} and 26.75 ^{o}C, respectively. The latent heat and melting temperature of the nanoencapsulated PCM is 86.13 kJ·kg^{-1} and 20.60 ^{o}C, respectively. The core material mass ratio could be determined by [22, 24]:

$$\text{PCM content (\%)} = H_{nanoPCM}/H_{PCM} \times 100\% \quad (10)$$

where $H_{nanoPCM}$ is the latent heat of nanoencapsulated PCM, H_{PCM} is the latent heat of only core material. The calculated PCM content in the nanoencapsulated PCM by DSC result is 41.59%, and by DPD simulation, is 47.61%. There are two main reasons to explain the difference of experimental results and DPD simulated results. The first reason is that the diameter of nanoencapsulated PCM may effected by the stirring rate and the amount of surfactant. In addition, the molar volumes and solubility parameters in the DPD simulation are obtained by the MD method, which performed on the basis of statistical mechanics, that a more accurate force field need to be

further improved for MD simulations. However, the DPD method used to fabricate the nanoencapsulated PCM is worthwhile to further study.

4. Conclusions

To understand the morphologies and evolution mechanisms of the thermal energy storage nanoencapsulated PCM in mesoscopic, the coarse-grained models of the n-octadecane-based nanoencapsulated PCM system were constructed. The DPD simulations were calculated with periodic boundary conditions. Coupled with the DPD simulation, the experiment was performed to prepare the PCM capsules. The main conclusions are summarized as follows according to the DPD simulation and experiment:

(1) The nanoencapsulated PCM were successfully fabricated based on the coarse-grained models by using DPD simulation method. The used n-octadecane as alkane was encapsulated clearly by the shell materials.

(2) Based on the feasible encapsulated structure, the PCM capsules were prepared by using experiment method. The average diameter of the prepared PCM capsules is 48.80 nm.

(3) The latent heat and melting temperature of the prepared nanoencapsulated PCM is 86.13 $kJ \cdot kg^{-1}$ and 20.60 ^{o}C, respectively. And the alkane content in the nanoencapsulated PCM is 41.59%.

(4) The alkane content in the nanoencapsulated PCM by DPD simulation is 47.61%, the difference indicated that many worthwhile work need to be further done.

Acknowledgements

This work was supported by the Fundamental Research Funds for the Central Universities

(China University of Mining and Technology, No. 2014QNA24) and the Open Fund Program of Key Laboratory of Efficient Utilization of Low and Medium Grade Energy (Tianjin University), Ministry of Education of China (2014-4302).

References

[1] J. M. Khodadadi, L. Fan and H. Babaei, Renew. Sust. Energ. Rev., 2013, 24, 418-444.

[2] P. Tatsidjodoung, N. Le Pierrès and L. Luo, Renew. Sust. Energ. Rev., 2013, 18, 327-349.

[3] T. Nomura, N. Okinaka and T. Akiyama, Resour Conserv Recy, 2010, 54, 1000-1006.

[4] M. K. Rathod and J. Banerjee, Renew. Sust. Energ. Rev., 2013, 18, 246-258.

[5] F. Pitié, C. Y. Zhao and G. Cáceres, Energy Environ. Sci., 2011, 4, 2117-2124.

[6] Y. Tian and C. Y. Zhao, Appl. Energy 2013, 104, 538-553.

[7] M. Li and Z. Wu, Renew. Sust. Energ. Rev., 2012, 16, 2094-2101.

[8] M. Liu, W. Saman and F. Bruno, Renew. Sust. Energ. Rev., 2012, 16, 2118-2132.

[9] L. W. Fan and J. M. Khodadadi, Renew. Sust. Energ. Rev., 2011, 15, 24-46.

[10] F. Kuznik, D. David, K. Johannes and J.-J. Roux, Renew. Sust. Energ. Rev., 2011, 15, 379-391.

[11] A. Waqas and Z. Ud Din, Renew. Sust. Energ. Rev., 2013, 18, 607-625.

[12] Z. H. Rao, S. F. Wang and Z. G. Zhang, Renew. Sust. Energ. Rev., 2012, 16, 3136-3145.

[13] N. Sarier and E. Onder, Thermochim. Acta 2012, 540, 7-60.

[14] Z. H. Rao and S. F. Wang, Renew. Sust. Energ. Rev., 2011, 15, 4554-4571.

[15] P. B. Salunkhe and P. S. Shembekar, Renew. Sust. Energ. Rev., 2012, 16, 5603-5616.

[16] N. Calvet, X. Py, R. Olivès, J.-P. Bédécarrats, J.-P. Dumas and F. Jay, Energy, 2013, 55, 956-964.

[17] J. P. Wang, X. X. Zhang and X. C. Wang, Renewable Energy 2011, 36, 2984-2991.

[18] Y. Hong, S. Ding, W. Wu, J. Hu, A. A. Voevodin, L. Gschwender, E. Snyder, L. Chow and M. Su, ACS Appl. Mater. Interfaces 2010, 2, 1685-1691.

[19] G. H. Zhang, S. A. F. Bon and C. Y. Zhao, Sol. Energy 2012, 86, 1149-1154.

[20] Y. Fang, S. Kuang, X. Gao and Z. Zhang, Energy Convers. Manage., 2008, 49, 3704-3707.

[21] X. X. Zhang, Y. F. Fan, X. M. Tao and K. L. Yick, Mater. Chem. Phys., 2004, 88, 300-307.

[22] G. Fang, H. Li, F. Yang, X. Liu and S. Wu, Chem. Eng. J., 2009, 153, 217-221.

[23] M. G. Li, Y. Zhang, Y. H. Xu and D. Zhang, Polym. Bull., 2011, 67, 541-552.

[24] Z.-H. Chen, F. Yu, X.-R. Zeng and Z.-G. Zhang, Appl. Energy 2012, 91, 7-12.

[25] Z. H. Rao, S. F. Wang, F. F. Peng, W. Zhang and Y. L. Zhang, Energy, 2012, 44, 805-812.

[26] R. D. Groot and P. B. Warren, J. Chem. Phys., 1997, 107, 4423-4435.

[27] P. Espanol and P. Warren, Europhys. Lett., 1995, 30, 191-196.

[28] G. H. Hu, J. G. Gai, H. L. Li, S. P. Zhu and S. Hoppe, Ind Eng Chem Res, 2010, 49, 11369-11379.

[29] Y. Qian, X. D. Guo, J. P. K. Tan, S. H. Kim, L. J. Zhang, Y. Zhang, J. L. Hedrick and Y. Y. Yang, Biomaterials, 2009, 30, 6556-6563.

[30] Z. H. Rao, S. F. Wang and F. F. Peng, Int. J. Heat Mass Transfer 2013, 66, 575-584.

[31] Z. H. Rao, S. F. Wang and F. F. Peng, Int. J. Heat Mass Transfer 2013, 64, 581-589.

[32] Z. H. Rao, S. F. Wang and F. F. Peng, Appl. Energy 2012, 100, 303-308.

Figure Captions:

Fig. 1 Coarse-grained models of water (a), n-octadecane (b), methyl methacrylate (c), methyl acrylate (d), azodiisobutyronitrile (e), sodium dodecyl sulfate (f)

Fig. 2 Energy and density fluctuating of methyl methacrylate

Fig. 3 Pressure, temperature and diffusivity evolution with simulated time

Fig. 4 Density concentration profiles and stress difference in the nanoencapsulated PCM system

Fig. 5 The morphology of a capsule at t=200000 steps from the DPD simulations

Fig. 6 Change of aggregates with increasing simulation steps: (a) 0 step, (b) 2000 step, (c) 20000 step, (d) 100000 step, (e) 150000 step, (f) 200000 step

Fig. 7 The SEM image and particle size distribution of the nanoencapsulated PCM by experiment

Fig. 8 DSC curves of the nanoencapsulated PCM and the core material

Table 1 The molar volumes and solubility parameters of beads

Table 2 The interaction parameters of beads in the PCM system

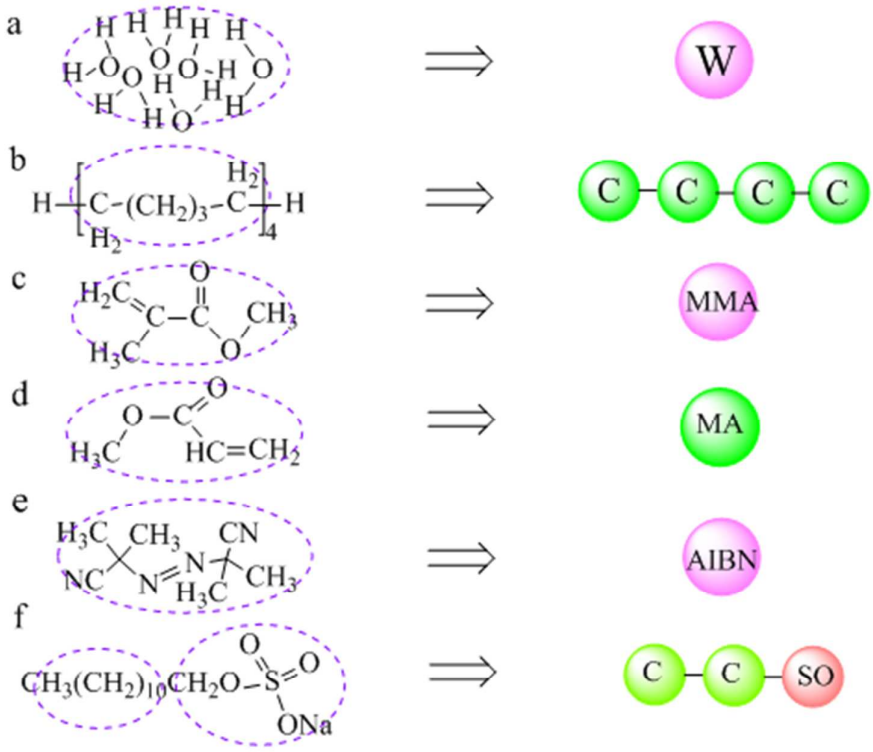

Fig. 1 Coarse-grained models of water (a), n-octadecane (b), methyl methacrylate (c), methyl acrylate (d), azodiisobutyronitrile (e), sodium dodecyl sulfate (f)

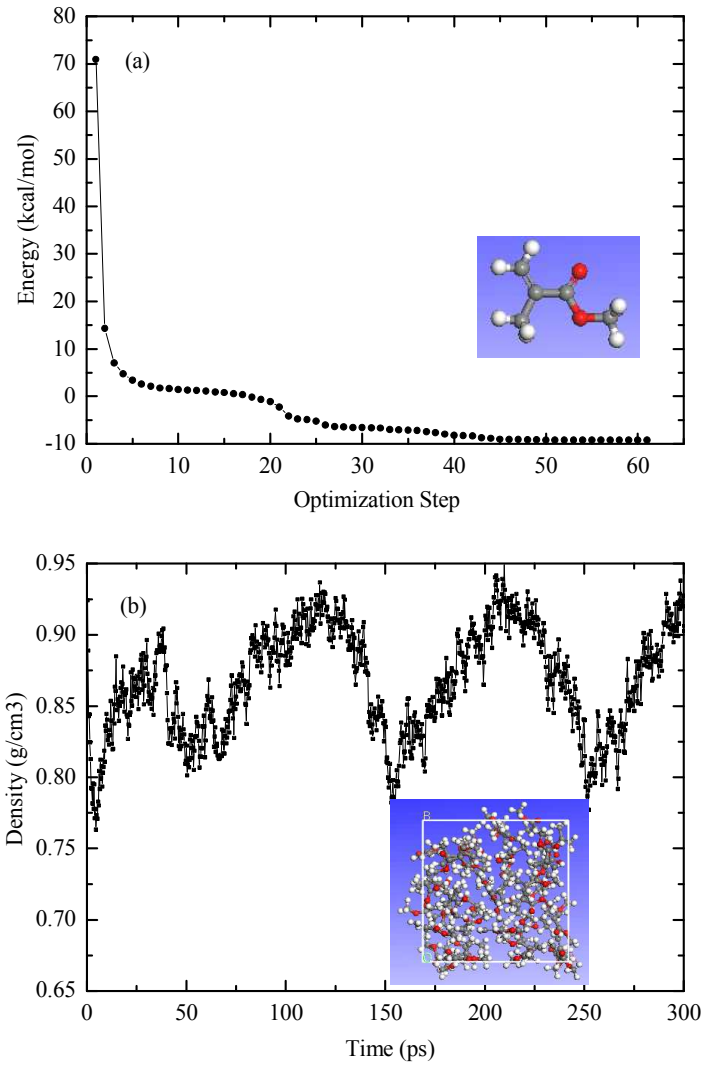

Fig. 2 Energy and density fluctuating of methyl methacrylate

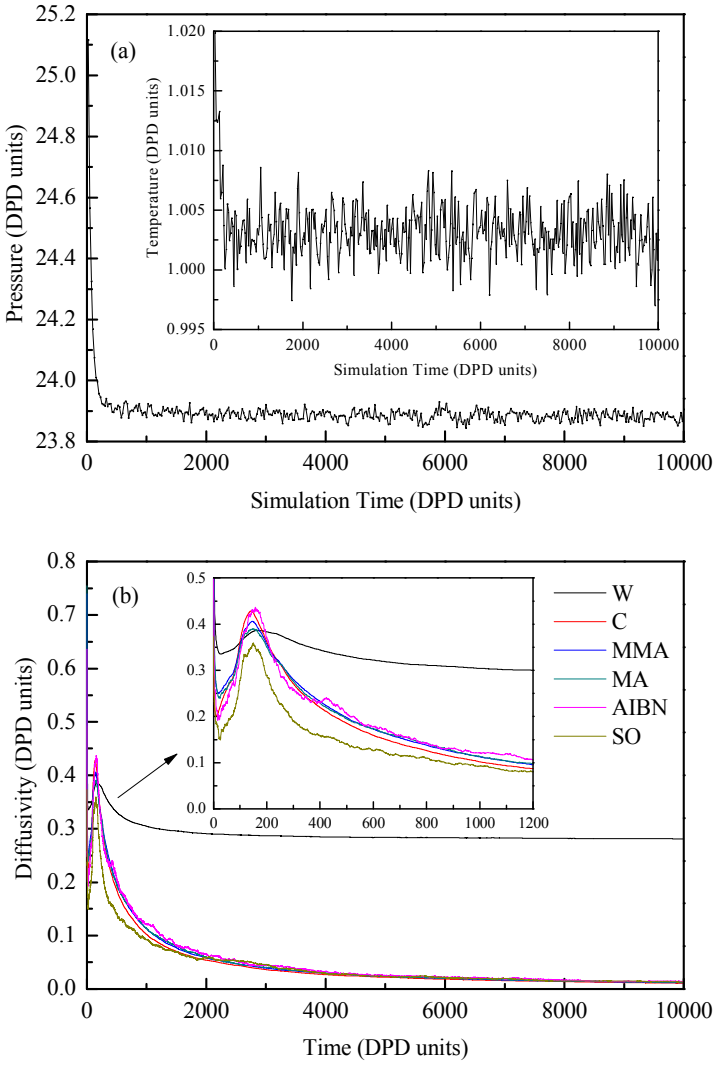

Fig. 3 Pressure, temperature and diffusivity evolution with simulated time

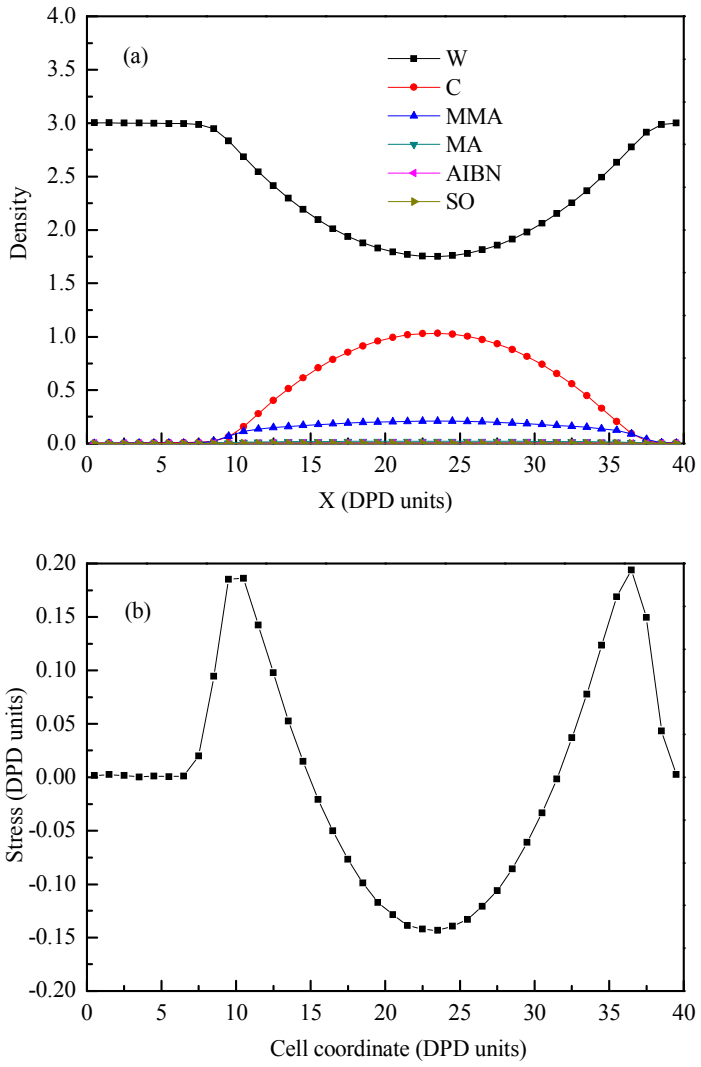

Fig. 4 Density concentration profiles and stress difference in the nanoencapsulated PCM system

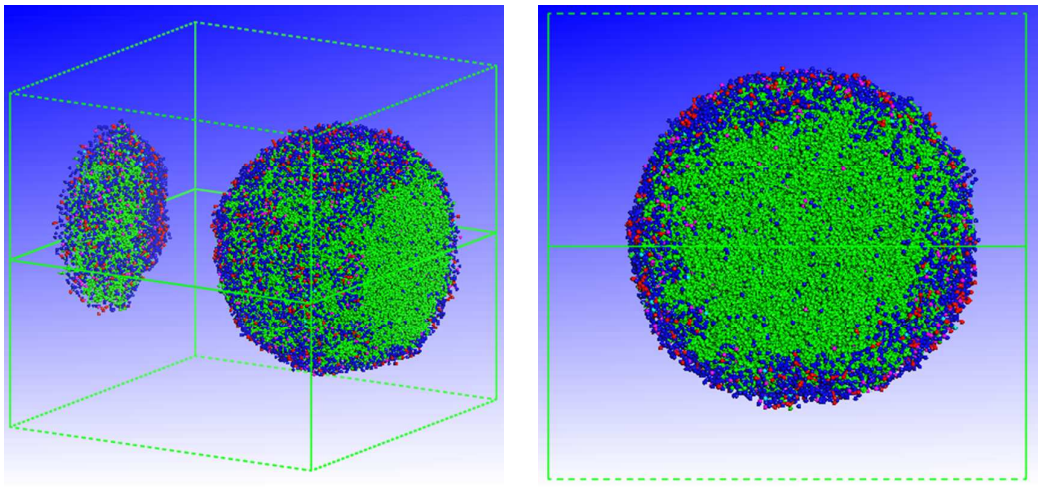

(C: ; MMA: ; MA:)

Fig. 5 The morphology of a capsule at *t*=200000 steps from the DPD simulations

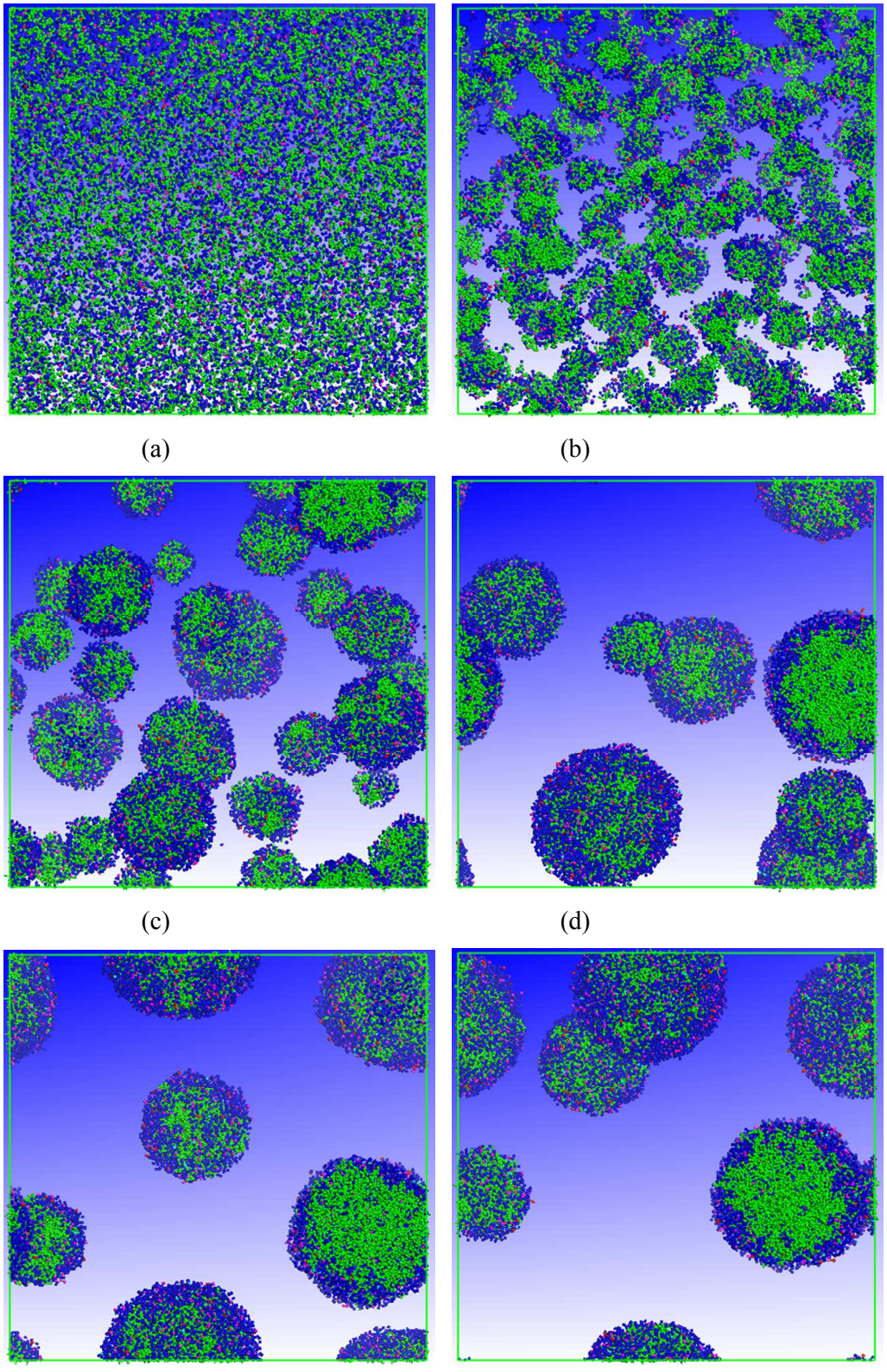

Fig. 6 Change of aggregates with increasing simulation steps: (a) 0 step, (b) 2000 step, (c) 20000 step, (d) 100000 step, (e) 150000 step, (f) 200000 step

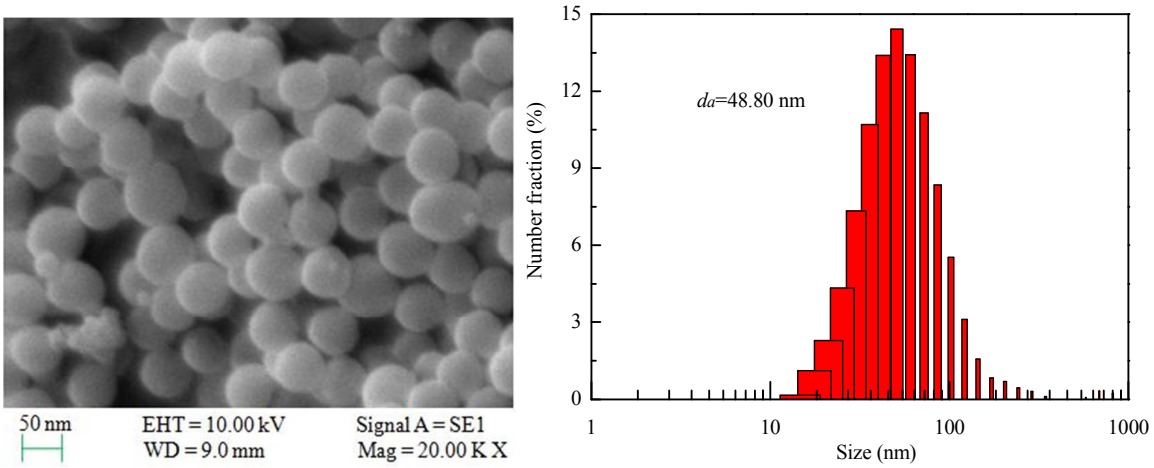

Fig. 7 The SEM image and particle size distribution of the nanoencapsulated PCM by experiment

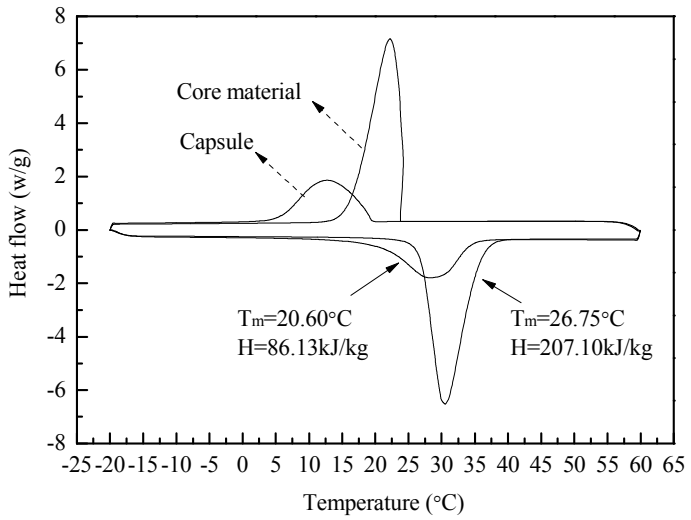

Fig. 8 DSC curves of the nanoencapsulated PCM and the core material

Table 1 The molar volumes and solubility parameters of beads

Bead	V_{bead} (cm^3 mol^{-1})	δ (J cm^{-3})
W	118.44	43.79
C	136.89	10.69
MMA	116.63	16.95
MA	100.43	17.38
AIBN	202.82	13.58
SO	78.34	24.69

Table 2 The interaction parameters of beads in the PCM system

Bead	W	C	MMA	MA	AIBN	SO
W	25					
C	185.39	25				
MMA	122.09	30.69	25			
MA	112.51	31.08	25.03	25		
AIBN	159.40	37.23	25.49	25.26	25	
SO	66.17	52.83	31.70	30.46	30.95	25